Structural and Orientational Properties of the Ferro, Antiferroelectric, and Re-entrant Smectic C* Phases of ZLL7/* by Deuterium NMR and Other Experimental Techniques

Donata Catalano,[†] Valentina Domenici,[†] Alberto Marini,[†,‡] and Carlo Alberto Veracini*[,†]

Dipartimento di Chimica e Chimica Industriale, Università degli Studi di Pisa, via Risorgimento 35, 56126 Pisa, Italy, and Scuola Normale Superiore di Pisa, Piazza dei Cavalieri 7, 56126 Pisa, Italy

Alexej Bubnov[§] and Milada Glogarová[§]

Institute of Physics, Academy of Sciences of the Czech Republic, Na Slovance 2, 182 21 Prague, Czech Republic

Received: April 7, 2006; In Final Form: June 27, 2006

In this work, two selectively deuterium-labeled isotopomers of the (*S*)-2-methylbutyl- [4′-(4″-heptyloxyphenyl)-benzoyl-4-oxy-(*S*)-2-((*S*)-2′)-benzoyl)-propionyl)]-propionate (**ZLL 7/***), one labeled on the phenyl ring (**ZLL 7/*-phe-D2**) and the other one on the biphenyl fragment (**ZLL 7/*-biphe-D2**), have been investigated by deuterium NMR (DNMR) spectroscopy and other experimental techniques. These compounds possess the paraelectric SmA, the ferroelectric SmC*, the antiferroelectric SmC*$_A$, the re-entrant ferroelectric SmC*$_{re}$, and the ferroelectric *hexatic* phases down to room temperature. The orientational ordering properties of the two labeled fragments have been determined by means of DNMR, and the mesophase behavior at two magnetic fields is discussed. In particular, the effect of the magnetic field on the supramolecular structure of the SmC* and SmC*$_{re}$ phases is commented. This study revealed to be useful to understand the structural and conformational properties of the ferroelectric/antiferroelectric/re-entrant/hexatic smectic phases. Mesomorphic properties, spontaneous tilt angle, polarization, and layer spacing have been studied for the labeled materials and compared with those obtained for the nonlabeled compound. The two self-consistent set of data, from optical and DNMR measurements and X-ray results, allow us to associate at the transition from the SmC* to the SmC*$_A$ phase a change of the molecular conformation.

Introduction

Chiral liquid crystalline smectogens with ferroelectric and antiferroelectric phases represent a very interesting class of compounds because of their promising technological applications.[1] After the discovery of the first antiferroelectric chiral smectic phase (SmC*$_A$) in the MHPOBC liquid crystal,[2] many new materials have been synthesized in attempt to study the detailed structure of this mesophase. In this research effort, one of the most interesting results in the recent years is the identification of several subphases, including the so-called SmC*$_A$ and the *ferrielectric* phases SmC*$_{FI1}$ and SmC*$_{FI2}$.[3] Moreover, below the antiferroelectric phase (SmC*$_A$), which appears on decreasing the temperature from more fluid smectic phases, highly ordered phases can exist, called *hexatic* phases, such as the tilted SmI*, SmI*$_A$, and SmF* phases, showing a long-range orientational order.[4] Less commonly found are the re-entrant phases, which are known to appear in the presence of electric or magnetic fields but also in the absence of any external constraints, as in the case under study. The re-entrant nematic (N_{re}) phase is more common,[5] while the re-entrant smectic (SmC*$_{re}$) phase has been found only with two pure compounds[6,7] and in mixtures.[8] The N_{re} phase was included in the more general class of frustrated phases.[9] On the basis of the Landau free energy, the appearance of SmC*$_{re}$ phase was explained as the result of increased quadrupolar ordering, which could change the interaction between molecules in neighboring layers.[6]

Generally, the links between mesomorphic behavior and compositional, structural, and dynamic properties at a molecular level are fundamental and at the moment far from complete understanding.[10] For the materials investigated in this work,[8] which exhibit a rich variety of mesophases, including the SmC*$_{re}$ phase, any data on molecular dynamics and orientational ordering are missing. The synthesis and physical properties of the compound denoted as **ZLL 7/*** have been already presented in ref 7. Besides, variants labeled by deuterium on the phenyl ring and on the biphenyl moiety have been synthesized,[11] which enable NMR study of particular molecular fragments.

Nuclear magnetic resonance (NMR) has been largely applied to the investigation of structure, orientational ordering,[12] and dynamics[13,14] of low-molecular-weight achiral liquid crystals and, more recently, has been revealed to be very effective for similar studies on chiral liquid crystals.[15]

Deuterium NMR (DNMR) spectroscopy is particularly powerful due to the intramolecular nature of the dominant quadrupolar interaction, allowing a quite straightforward interpretation of both static spectra and relaxation measurements and providing structural and dynamic site-specific information. Even though the use of DNMR is strongly limited by the requirement of purposely and selectively ^{2}H labeled molecules, DNMR has

* Author for correspondence. E-mail: verax@dcci.unipi.it. Telephone: +39-0502219235. Fax: +39-0502219260.
† Dipartimento di Chimica e Chimica Industriale, Università degli Studi di Pisa.
‡ Scuola Normale Superiore di Pisa.
§ Institute of Physics, Academy of Sciences of the Czech Republic.

10.1021/jp0621777 CCC: $33.50
Published on Web 07/29/2006

SCHEME 1: Molecular Structure of ZLL 7/* (X=Y=H) and the Two Isotopomers ZLL 7/*-phe-D2 (X=D, Y=H) and ZLL 7/*-biphe-D2 (X=H, Y=D)

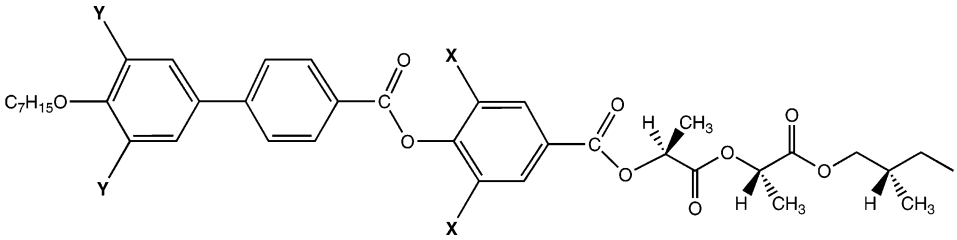

TABLE 1: Sequence of Phases, Melting Points mp [°C] on First Heating, Transition Enthalpies ΔH [J g^{-1}], and Phase Transition Temperatures [°C] from DSC Measured on Cooling at a Rate 5 K min^{-1} for Indicated Compounds

	mp	Cr		hex		SmC*$_r$		SmC*$_A$		SmC*		SmA		iso
ZLL 7/*	61		54		65		71		98		104		129	
		•		•		•		•		•		•		•
	[+17.6]		[−12.3]		[−2.2]		[−0.06]		[−0.04]		[−0.19]		[−5.7]	
ZLL 7/*-phe-D2	61		51		64		70		95		101		128	
		•		•		•		•		•		•		•
	[+12.5]		[−11.6]		[−2.0]		[−0.05]		[−0.03]		[−0.18]		[−5.6]	
ZLL 7/*-biphe-D2	59		50		62		69		93		98		127	
		•		•		•		•		•		•		•
	[+13.5]		[−12.0]		[−2.2]		[−0.05]		[−0.03]		[−0.19]		[−6.2]	

been used to characterize several ferroelectric compounds as 11EB1M7,[16,17] MBHB, [18,19] and 8BEF5,[20−22] as well as antiferroelectric mesogens, as 10B1M7.[23,24]

The case reported here is quite original because it is the first characterization of a re-entrant smectic phase by means of DNMR. By analyzing the line-shape of deuterium NMR spectra in the SmC* and SmC*$_{re}$ phases, a hypothesis of the structure of the mesophases under the effect of the magnetic field can also be drawn. In fact, the smectogen studied shows a peculiar behavior at two different values of the magnetic field. This effect, which determines the unwinding of the chiral helix in the SmC* phase, is discussed in terms of free energy of the bulk, referring to the phenomenological model reported in ref 25. Further elements of interest are the investigation of the ordering properties of the antiferroelectric, re-entrant, and hexatic phases. The changes of the line-width within the various mesophases are also discussed, and they confirm the significant differences in the dynamic processes between the ferro- and antiferroelectric phases, as previously found for another smectogen.[24]

The paper is organized as follows: The first part is devoted to the characterization of labeled materials and comparison of mesomorphic properties, spontaneous tilt angle, and polarization and layer spacing of labeled compounds with those of the nonlabeled one studied previously.[7] This part is followed by the DNMR study of both labeled compounds with detailed discussion, and conclusions are drawn in the final part of the paper, where the evidence of a conformational change of the molecule passing through the SmA−SmC*−SmC*$_A$ phases has been discussed.

Experimentals and Results

Materials and their Characterization. The structure of the compounds studied in this paper is presented in Scheme 1: nondeuterated (**ZLL 7/***), deuterated on phenyl ring (**ZLL 7/*-phe-D2**), and deuterated on biphenyl moiety (**ZLL 7/*-biphe-D2**). The compounds have the following molecular structure: nonchiral alkyl chain, molecular core (biphenyl connected to phenyl by an ester group), and chiral chain with three chiral centers connected to the core and one to another by the ester groups. Synthesis details are presented in ref 7 for nonlabeled compound and in ref 11 for the deuterated ones. Both synthetic routes followed were stereospecific, and the chiral reagents used presented more than 99% (*S*) configuration. Therefore, the final products should show consequently high stereochemical purity. HPLC analyzes of the three compounds have shown a satisfactory and comparable purity level for **ZLL 7/***, **ZLL7/*-phe-D2** and **ZLL7/*-biphe-D2** samples.

Macroscopic properties of the nonlabeled **ZLL 7/*** were studied in detail and reported in refs 7 and 8. The labeled compounds were characterized by the same methods and procedures. Results of characterization and comparison of properties of nonlabeled and labeled compound are presented below.

Mesomorphic Properties. The sequence of phases and phase transition temperatures were determined from characteristic textures and from their changes observed in a polarizing microscope on cooling the sample from the isotropic phase. The transition temperatures were also checked by DSC (see Table 1), using a Pyris Diamond Perkin-Elmer 7 instrument with a cooling and heating rate of 5 K min^{-1}. Possible undercooling large effects can be excluded by considering the slow cooling (and heating) rate used and the overall agreement with the transition temperatures found by other techniques, as described in the following. The labeled compounds possess the same mesophase sequence as the nonlabeled one:[7] paraelectric SmA, ferroelectric SmC*, antiferroelectric SmC*$_A$, ferroelectric SmC*$_{re}$, and ferroelectric hexatic (SmI* or SmF*), down to the crystalline phase. The phase transition temperatures as well as the stability range of the mesophases of the three studied compounds are slightly different. However, the temperature differences exceed 3 °C only when **ZLL7/*** and **ZLL 7/*-biphe-D2** are compared and only for the SmA−SmC* and SmC*−SmC*$_A$ transitions. Altogether, these differences can be ascribed to the deuteration itself or to minor impurities.

Polarization and Tilt Angle Measurements. Temperature dependences of spontaneous polarization (P_s) and spontaneous tilt angle (θ_s) have been measured for labeled compounds as done for nonlabeled ones.[7] The values of P_s have been evaluated from a $P(E)$ hysteresis loop detected during P_s switching in an

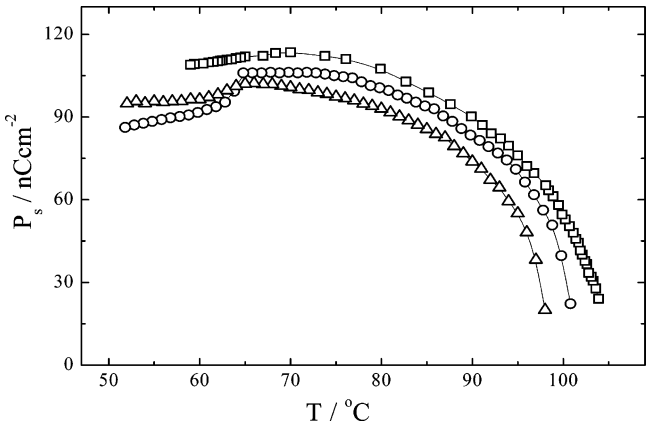

Figure 1. Temperature dependence of the spontaneous polarization measured on cooling for ZLL 7/* (□),[7] ZLL 7/*-phe-D2 (○), and ZLL 7/*-biphe-D2 (△).

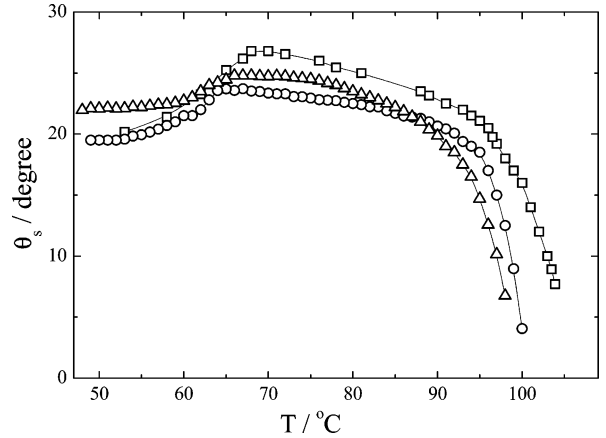

Figure 2. Temperature dependence of the spontaneous tilt angle measured optically on cooling for ZLL 7/* (□),[7] ZLL 7/*-phe-D2 (○), and ZLL 7/*-biphe-D2 (△).

ac electric field E of frequency 60 Hz. The values of θ_s have been determined optically from the difference between extinction positions detected at crossed polarizers under opposite dc electric fields ± 40 kVcm^{-1}. The results are shown in Figures 1 and 2, respectively, together with data of the nonlabeled compound for comparison. For labeled compounds, the temperature dependences of both quantities exhibit the same features as those of nonlabeled one,[7] confirming that the character of the phase transitions is not affected by deuteration. The decrease of P_s values at the transition to the hexatic phase is more rapid for deuterated compounds and strictly resembles the typical decrease of other compounds in the homologue series ZLL.[7] The lowering of absolute values of both quantities with deuteration is small (about 15% at 75 °C) but systematic. As in previous works,[7,8] the temperature dependences of P_s and θ_s do not put in evidence the transitions SmC*−SmC*$_A$ and SmC*−SmC*$_{re}$.

Layer Spacing Data. Layer spacing (d) of **ZLL7/*-phe-D2** has been measured by X-ray diffraction on nonaligned samples by the same technique used for the nonlabeled material. [7] The results are shown in Figure 3. The variation of the layer spacing across all phases is qualitatively the same for the nonlabeled and labeled compounds, but the layer spacing is systematically greater in the case of the labeled material.

In the SmA phase, d slightly increases on cooling as a consequence of the increasing orientational order. The typical decrease of d at the onset of the SmC* is due to the tilt of the molecules in the smectic layers, and the small jump down at the transition to the SmC*$_A$ phase can be connected with a small,

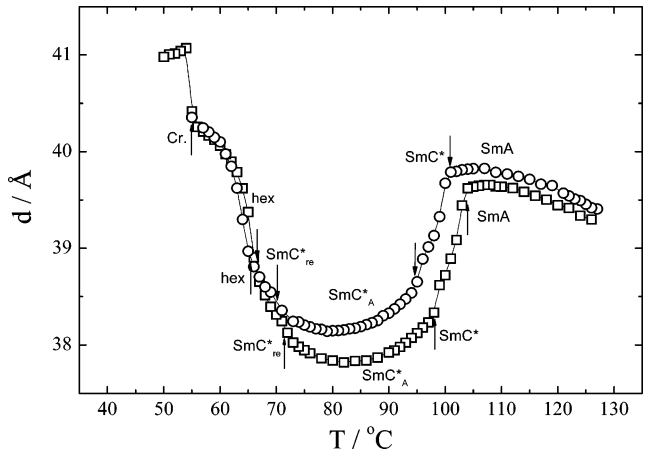

Figure 3. Temperature dependence of the layer spacing for ZLL 7/* (□)[7] and ZLL 7/*-phe-D2 (○). Phases and phase transition temperatures (arrows) are indicated.

sudden increment of the tilt angle in this phase. The onset of the SmC*$_{re}$ phase is hardly revealed by another slight discontinuity in the temperature dependence of the layer spacing. Because the tilt angle should not substantially decrease across the SmC* phases, the marked increase of d in the SmC*$_A$ and SmC*$_{re}$ phases on cooling is ascribed to the stretching of the aliphatic chains and to the related increase of the orientational order. On the other hand, the steep increment of d in the hexatic phase must reflect both the decrease of the tilt angle and the increase of the orientational order.[7]

Deuterium NMR Studies. *Experimental.* DNMR experiments were performed by using two NMR spectrometers working at different magnetic fields. Various sequences of spectra of both deuterated compounds were carried out on a 7.05 T Varian VXR-300 spectrometer, working at 46.04 MHz for deuterium. The spectra were acquired with a single pulse sequence, with a 90° pulse of 12 μs, a delay of 0.3 s, and 500−5000 scans.

A second set of DNMR experiments was carried out on both isotopomers using a 9.40 T Varian Infinity Plus 400 double-channel spectrometer operating at the deuterium frequency of 61.38 MHz, equipped with a goniometric probe for recording static spectra. These spectra were acquired by using the quadrupolar echo sequence [26] and a 90° pulse of 4.5 μs, a pulse delay of 1 s, a quadrupolar echo delay (τ) of 25 μs and 500 scans.

In both cases, the samples were microscopically aligned within the magnet by slow cooling from the isotropic phase and the spectra were recorded in steps of 1−4 °C. The temperature was stable within 0.2 °C. Because different cooling (and heating) rates and temperature equilibration times have been applied in each experiment, these parameters will be given in the following, whenever relevant to the discussion.

Data Analysis. All DNMR data are processed by using the software of the Varian instrumentations (SpinSight 4.3.2 software for Sun microsystem workstation and Varian). Spectral parameters were analyzed mostly using the Mathematica 5.0 (Copyright 1988−2003, Wolfram Research, Inc.) software for PC. Simulations of the line-shapes of DNMR spectra were performed using the "Lequor" software [27] on a Unix platform.

Quadrupolar and Dipolar Splittings, Line Widths, and Line Shapes vs Temperature. Selected DNMR spectra acquired for the two isotopomers **ZLL 7/*-phe-D2** and **ZLL7/*-biphe-D2** in the temperature range between 130 and 50 °C, operating at 46.04 MHz, are reported in Figures 4 and 5, respectively. A

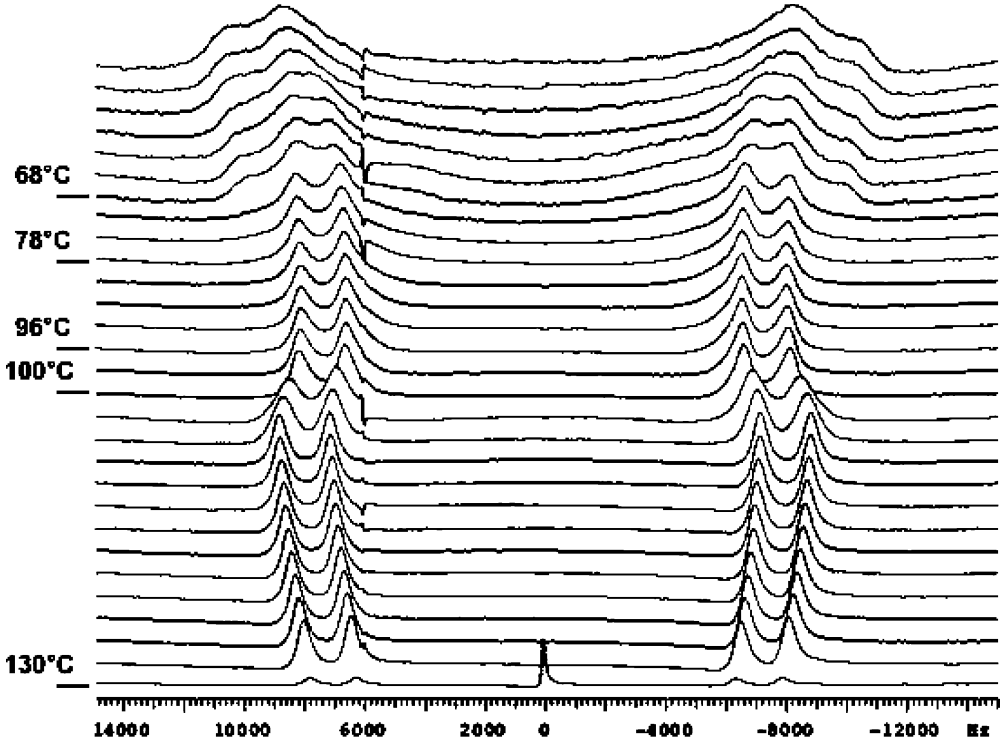

Figure 4. DNMR spectra of ZLL 7/*-phe-D2 recorded at variable temperature in the range 130−50 °C. The spectra, recorded without ^{1}H decoupling, show the D−H dipolar coupling.

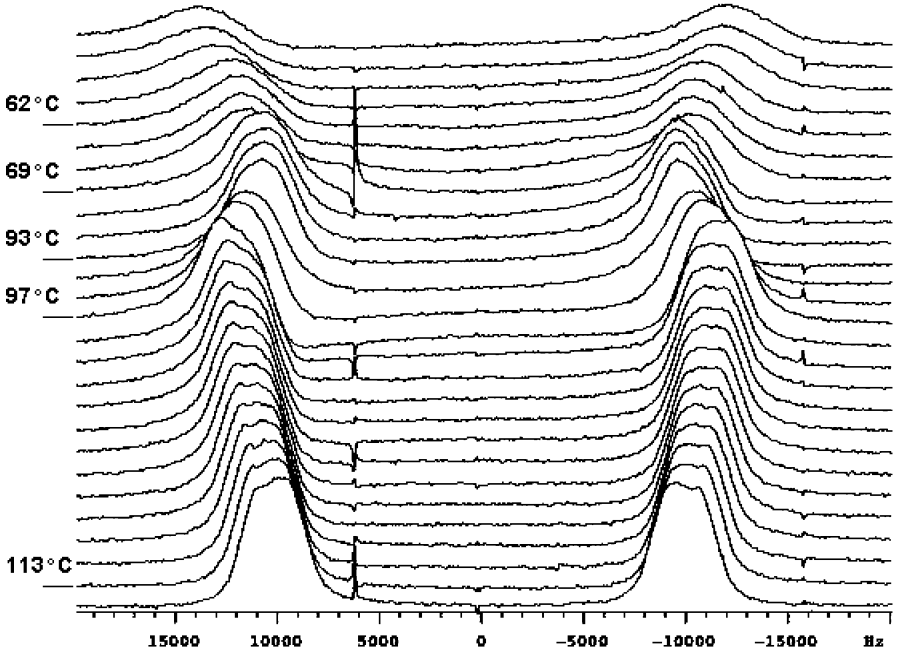

Figure 5. DNMR spectra of ZLL 7/*-biphe-D2 recorded at variable temperature in the range 135−50 °C. The spectra reported have been recorded without ^{1}H decoupling.

selection of DNMR spectra obtained under proton decoupling for the **ZLL7/*-biphe-D2** smectogen, at two magnetic fields, are reported in Figure 6.

In each compound, the two deuterons are equivalent as a result of the rapid rotation of the deuterated aromatic fragment around its para axis, and only one quadrupolar doublet is expected in the spectrum of liquid crystalline phases macroscopically aligned in the magnetic field. Each component of the doublet can be split into a further (typically much narrower) doublet by the dipolar interaction of the deuteron with a neighboring hydrogen (see Figure 4). This is the case of **ZLL 7/*-phe-D2**, where each deuteron shows a dominant dipolar interaction with the nearest aromatic proton. More complicated structures can arise from dipolar interactions with many hydrogen nuclei (see Figure 5), as happens for **ZLL7/*-biphe-D2**, where each deuteron dipolarly interacts with the nearest aromatic proton and with the first methylenic protons of the alkoxylic chain.

A suitable ^{1}H decoupling procedure eliminates all dipolar ^{1}H−D interactions, producing simpler spectra. From the evolu-

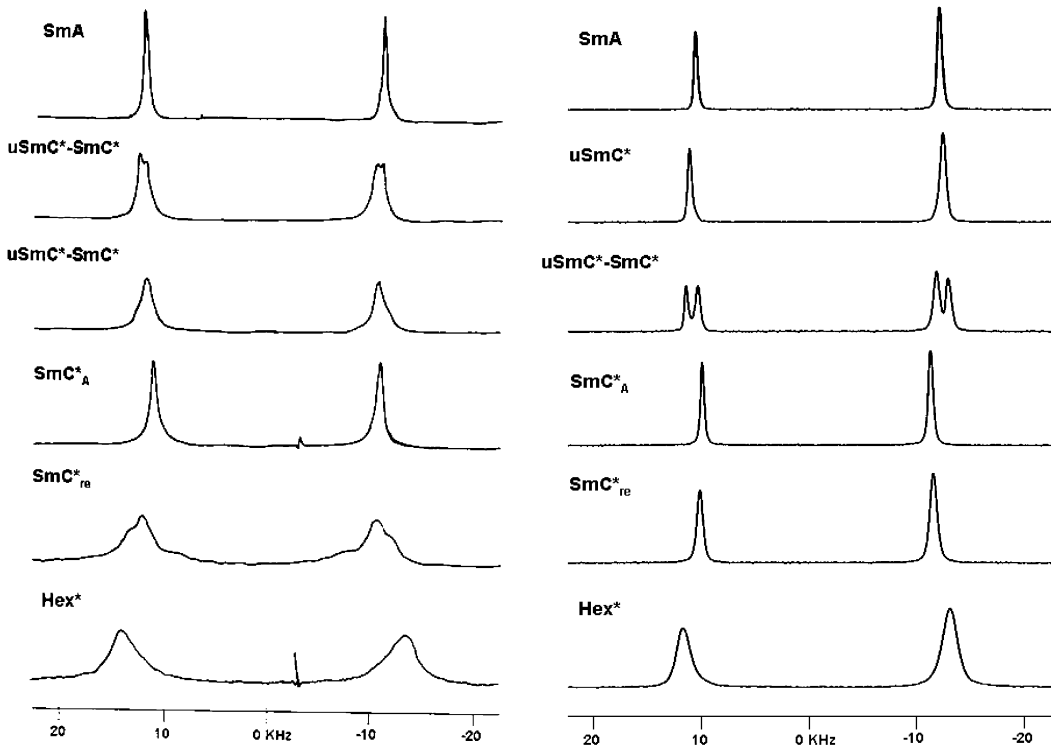

Figure 6. Selection of DNMR spectra of ZLL7/*-biphe-D2 in the SmA−uSmC*−SmC*−SmC*$_A$−SmC*$_{re}$−Hex phases (7.05 T on the left and 9.04 T on the right).

tion of the recorded spectra, with and without ^{1}H decoupling, with decreasing temperature, the mesomorphic behavior of the two samples can be recognized, essentially by the trends of the quadrupolar splittings, $\Delta\nu_q$, of the dipolar couplings, $\Delta\nu_{dip}$, and of the line widths or, more generally, line shapes. The phase transition temperatures correspond to discontinuities in these trends. For the compounds studied here, the transition temperatures found by DNMR agree within ±1 °C with those recorded by DSC, reported and discussed in the previous section.

The quadrupolar splittings of **ZLL 7/*-biphe-D2** and **ZLL 7/*-phe-D2** versus temperature are reported in Figure 7a and b, respectively, for the whole temperature range studied. The trends of $\Delta\nu_q$ versus temperature are quite similar for the two compounds, as can be seen from Figures 4, 5, and 7a,b. Also, the line shape features of the decoupled spectra, reported in Figure 6 for each mesophase for the sole **ZLL7/*-biphe-D2**, are similar for the two isotopomers so that the following presentation applies to both compounds: (1) In the SmA phase, the quadrupolar splittings $\Delta\nu_q$ regularly increase with decreasing temperature due to the increasing orientational order for both deuterated compounds. The trends of $\Delta\nu_q$ relative to the two different magnetic fields are practically superimposed. (2) The transition from the SmA to the SmC* phase is marked by a sudden increase of the line width (a usual feature) and by the unusual occurrence of a doubling of the signals (see Figures 6, 7, and 8). This indicates a biphasic situation, whose thermodynamical stability will be examined later. The two quadrupolar doublets have different intensities.

SCHEME 2: Structure of the SmC* and Unwound SmC* Phases in Presence of the External Magnetic Field H; *n* Is the Local Phase Director and l Is the Normal to the Smectic Plane (π)

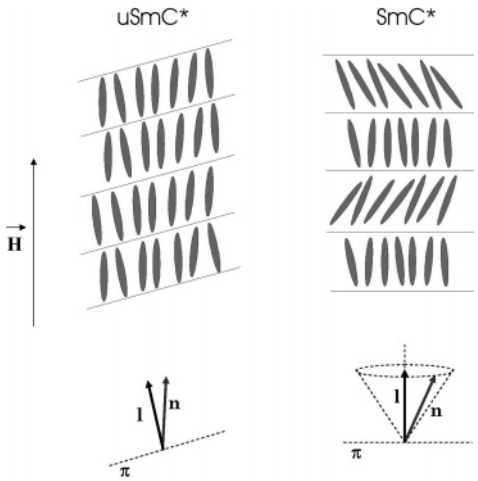

By lowering the temperature, the smaller splitting decreases and the greater increases; moreover, the outer signals lose intensity to the advantage of the inner ones. The couple of signals with smaller splitting is easily assigned to deuterons in a SmC* phase with the helix axis parallel to the magnetic field and the local director (long molecular axes average direction) tilted with respect to it. The couple of signals with larger splitting cannot be ascribed to the residual supercooled SmA phase because, below the phase transition, this splitting does not continue the trend followed in the SmA phase: in effect, the new trend seems to reveal the presence of SmC* phase unwound by the magnetic field (uSmC*), with the local director aligned along it (see Scheme 2). This interpretation is supported by the comparison with the data reported in ref 25, where a ferroelectric liquid crystal, showing SmA, SmC*, and SmF* phases, is studied by DNMR in three different magnetic fields: the helical structure survives in the lowest field, is unwound by the intermediate field only at high temperature, and is unwound by the most intense field at any temperature.

To verify the stability of the biphasic situation found, several sets of measurements have been performed by varying the equilibration time of the sample for each temperature and by cooling or heating the sample. These measurements can be

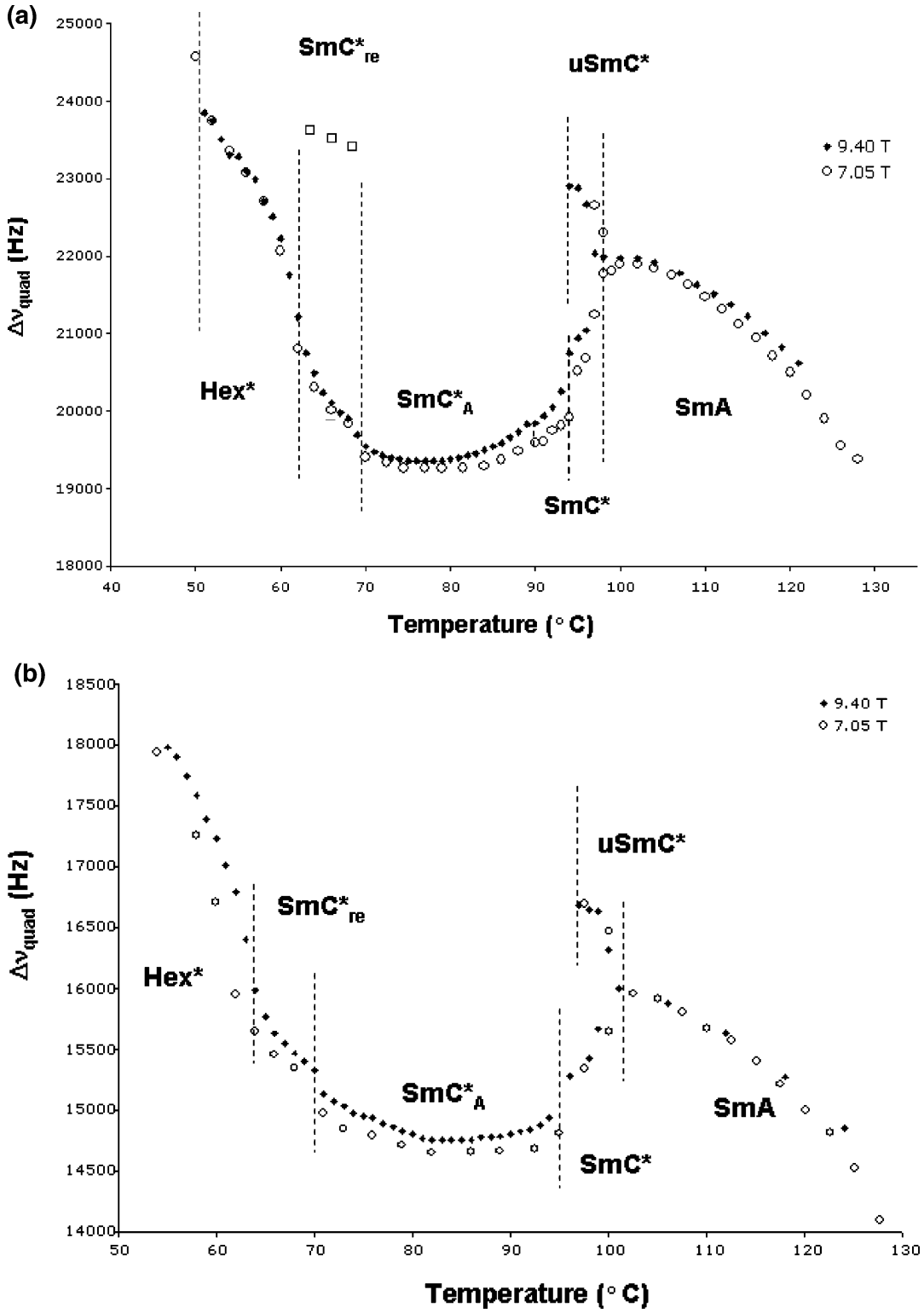

Figure 7. Quadrupolar splittings (Hz) vs temperature (°C) of the samples (a) ZLL 7/*-biphe-D2 and (b) ZLL 7/*-phe-D2, as obtained at two magnetic fields, namely 7.05 T (○) and 9.40 T (◆). For the ZLL 7/*-biphe-D2, Figure (a), quadrupolar splittings arising from the lateral peaks of the line-shape distribution in the reentrant smectic phase are also shown (□).

roughly divided into two groups, respectively, with short and long equilibration times (about 3 and 20 min, with temperature steps of 0.2 °C). As far as the measurements at 7.50 T are concerned, the spectra with short equilibration times recorded on cooling led to extended coexistence of unwound uSmC* and wound SmC* phases. In the second group of measurements, in which the mesogens had time enough to reach the most stable phase, the uSmC* phase hardly appears on cooling. The uSmC* phase never appears in the spectra recorded heating the sample. All this indicates that the phase thermodynamically stable just below the SmA one is the wound SmC* phase.

We examine now the phenomenon of efficiently unwinding the helix of the SmC* phase in the higher magnetic field. In Figure 8, a selection of the DNMR spectra of **ZLL7/*-biphe-D2** acquired at 9.40 T shows that here the uSmC* phase is stable in the temperature range of about 1−1.5 °C just below the

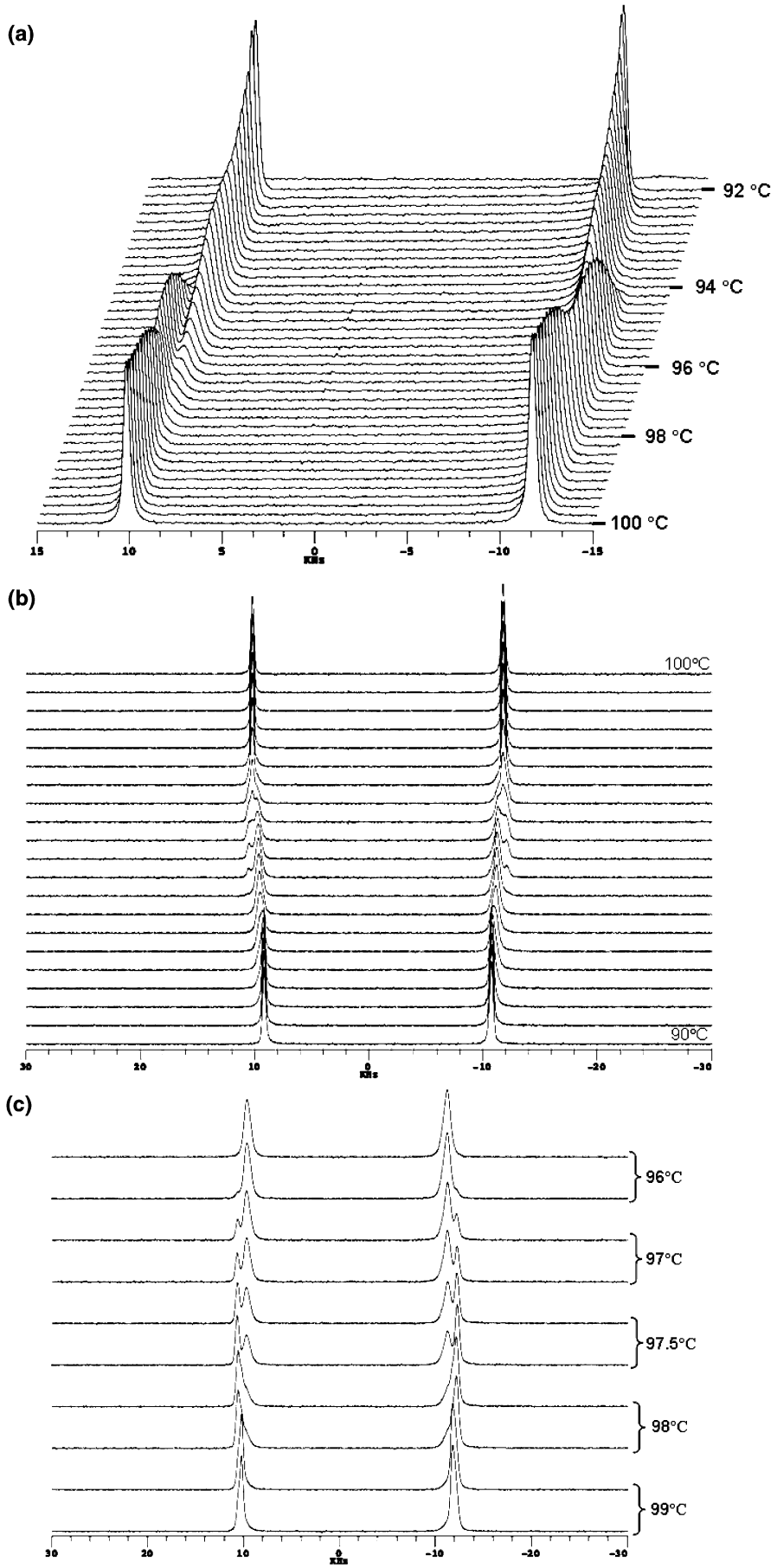

Figure 8. Selection of DNMR spectra of ZLL-biphe-D2 in the SmA−uSmC*−SmC* range recorded at 9.40 T. Here the effect of the cooling and heating procedures on phase occurrence is shown: (A) Spectra are recorded from 100 to 92 °C every 0.2 degrees (cooling). (B) Spectra are recorded from 90 to 100 °C every 0.5 degrees (heating). Figure C represents the evolution of spectra in time: spectra are acquired every 20 min. The spectra here reported show that the uSmC* is stable, for the ZLL-biphe-D2 smectogen, in the range 99−97.5 °C.

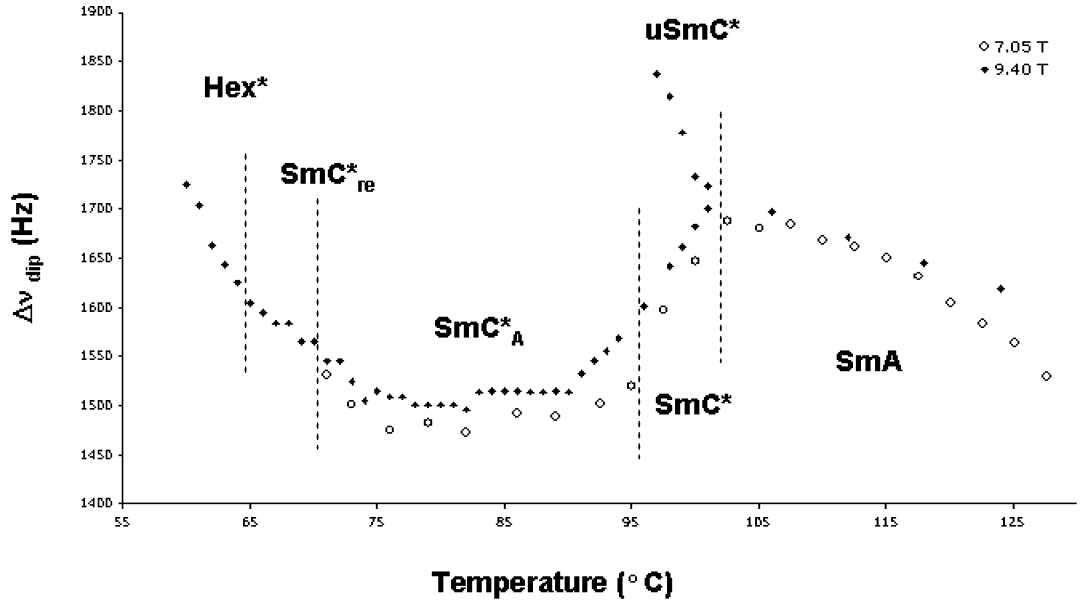

Figure 9. Dipolar splittings of the ZLL 7/*-phe-D2 in the SmA, SmC*, and SmC*$_A$ phases, obtained from DNMR spectra recorded at two magnetic fields, namely 7.05 T (□) and 9.40 T (●).

SmA−SmC* transition. In effect, in this temperature range, on cooling the sample, only the uSmC* phase exists, while on heating the sample from the SmC*$_A$, the wound and unwound phases coexist at first, but after about 30 min, when the sample reaches equilibrium, only the uSmC* remains. This fact confirms that the uSmC* phase is stable both on cooling and on heating in a narrow range of temperatures.

In the stable SmC* phase, a gradual decrease of the quadrupolar splittings of both compounds, in both magnetic fields, takes place, indicating a progressive tilt of the local directors with respect to the magnetic field. An interesting feature of the SmC* phase is the fact that there the spectral lines are larger than those in the SmA and uSmC* phases.

(1) The transition SmC*−SmC*$_A$ is put in evidence by the vanishing of any trace of uSmC* phase and by a small jump down of the quadrupolar splitting, which only very slightly decreases on cooling the SmC*$_A$ phase itself. Moreover, in this phase, the spectral lines are considerably narrower than in the SmC* one, indicating the absence of significant fluctuations of the magnetic field or a more homogeneous alignment of molecules within the layers rather than a quicker orientational averaging process.[24]

In effect, in the spectra recorded in the 7.05 T field, an asymmetry appears at the base of the lines, revealing a not completely averaged distribution of orientations inside the sample: this distribution may derive from a less-efficient exchange of molecules between the layers. Our findings agree with the behavior exhibited by similar AFLC compounds.[28]

(2) In the 7.05 T magnetic field, the onset of the re-entrant phase (SmC*$_{re}$) is characterized by a dramatic change of the line shape (see Figure 6). Beyond any doubt, such line shape reflects a distribution of orientations exchanged by relatively slow averaging processes. This distribution is stable at least for 24 h and is recorded both on cooling and heating the sample. In Figure 7, two splittings are reported: the minor one is between the maximum intensity points of such distribution, the major one is between its external limits. The trend of the minor splitting, even if increasing with decreasing temperature, recovers that found in the SmC* phase, indicating that we really are in a SmC*$_{re}$ phase. In the 9.40 T magnetic field, the situation is different: a sharp quadrupolar doublet is obtained, with signals as narrow as those found in the SmC* phase (700−800 Hz), indicating an efficient orientational averaging process and a sample homogeneously aligned by the intense magnetic field (see Figure 6). Notwithstanding the different line shapes, the quadrupolar splittings observed at 9.40 T and the small one at 7.05 T excellently superimpose, in particular in the case of **ZLL7/*-biphe-D2**; on decreasing temperature, they continuously increase, as is evident in Figure 7.

(3) On entering the *hexatic* phase, we observe, at 9.40 T, a quadrupolar doublet of very large signals (1200−1800 Hz) and, at 7.05 T, a distribution with intense maxima at its ends, between which we evaluate the quadrupolar splitting. Considering the quadrupolar splitting trends in the two magnetic fields, which are just coincident in the case of **ZLL7/*-biphe-D2**, a jump to higher values is observed at the transition SmC*$_{re}$−hexatic, followed by an almost linear trend within the phase.

Finally, we go back to the dipolar structures described at the beginning of this section. For **ZLL7/*-phe-D2** at the two magnetic fields, the splitting due to the dipolar coupling between the deuteron and the nearest aromatic proton, $\Delta\nu_{dip}$, is reported in Figure 9 as a function of temperature (such splitting is not resolved in the uSmC*, SmC*$_{re}$, and *hexatic* phases at 7.50 T). In the SmA phase, the dipolar splitting increases on cooling, while in the SmC* one, it rapidly decreases (in the uSmC* phase it, of course, increases), reaches a minimum value in the SmC*$_A$ phase, then increases again in the SmC*$_{re}$ phase. Altogether, its trend resembles that typical of the quadrupolar splittings of Figure 7, but it is affected by a much higher experimental relative error (about 3% instead of 0.4%).

As far as **ZLL 7/*-biphe-D2** is concerned, the complex, unresolved dipolar structure will be examined in the next section.

Orientational Order Parameters. From the values of the experimental quadrupolar and dipolar splittings, a quantitative evaluation of molecular order parameters has been performed.[12,13] In the following of this paper, the order parameters are always referred to the magnetic field direction except when specified otherwise. Moreover, all the computations reported are based on the spectral data sets determined at 9.04 T.

In the present cases, the order parameters experimentally accessible are relative to one deuterated aromatic ring in each molecule. The quadrupolar and dipolar splittings are connected

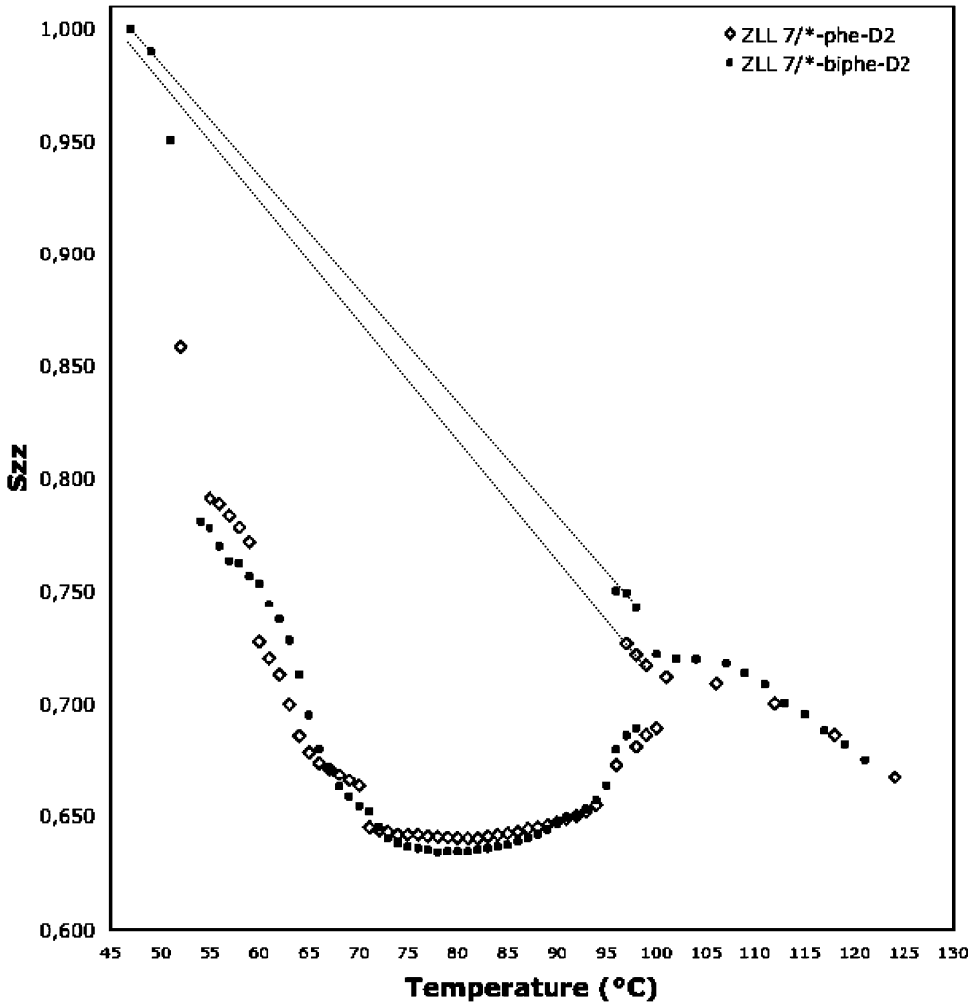

Figure 10. Order parameter S_{zz} of the two labeled ZLL 7/* compounds vs temperature (°C). Squares and rhombs refer to ZLL 7/*-biphe-D2 and ZLL 7/*-phe-D2, respectively.

to the order parameters $S_{zz}(T)$ and $\Delta_{biax}(T) = S_{xx}(T) - S_{yy}(T)$ of the deuterated ring by the following equations:[29]

$$\Delta\nu_{dip}(T) = -2K_{DH}\frac{S_{zz}(T)}{r_{DH}^3} \quad (1)$$

$$\Delta\nu_q(T) = \frac{3}{2}q_{aa}\left\{S_{zz}(T)\cdot\left(\cos^2\phi - \frac{1}{2}\sin^2\phi - \frac{\eta}{6}\cos^2\phi + \frac{\eta}{6} + \frac{\eta}{3}\sin^2\phi\right) + \Delta_{biax}(T)\left(\frac{1}{2}\sin^2\phi + \frac{\eta}{6}\cos^2\phi + \frac{\eta}{6}\right)\right\} \quad (2)$$

where $K_{DH} = \gamma_D\gamma_H h/4\pi^2 = 18\ 434.4$ Hz·Å^3, r_{DH} is the distance between the interacting nuclei, and q_{aa} and η are the quadrupolar coupling constant and asymmetry parameter, respectively. The standard values of $r_{DH} = 2.5$ Å, $q_{aa} = 185$ kHz, $\eta = 0.04$ have been used in the following. For para-disubstituted aromatic rings quickly rotating around the para axis, the principal reference frame of the order tensor has its x and z axes in the ring plane, with z along the para direction. The angle ϕ between the C−D bond and the z direction has been assumed equal to 60°.

From the experimental data relative to the two isotopomers studied, two sets of order parameters have been obtained for each magnetic field.

In the case of the **ZLL 7/*-phe-D2**, eqs 1 and 2 could be solved at each temperature to obtain $S_{zz}(T)$ and $\Delta_{biax}(T)$. However, because Δ_{biax} was always very small and poorly determined, it was decided to constrain its temperature dependence accordingly to the empirical relationship $\Delta_{biax}(T) = A + B^*T$, in each phase separately. Using this relation and eqs 1 and 2, all the available couples of experimental data were contemporarily fit, so determining the $S_{zz}(T)$ values and the parameters A and B. Best fitting S_{zz} values at the different temperatures are reported in Figure 10. The S_{zz} values relative to the hexatic phase, where no dipolar splitting was available, were determined using only the quadrupolar splittings and the values of A and B from the previous fitting. The values of Δ_{biax} range between 0.053 and 0.057 in the SmA, 0.055 and 0.048 in the SmC*, 0.046 and 0.038 in the SmC*$_A$, and again increase in the SmC*$_{re}$ and *hexatic* phases from 0.037 to 0.055.

In the case of **ZLL 7/*-biphe-D2**, because the dipolar splittings were unresolved but contained in the line shape, we performed the simulation of the ^{1}H-coupled DNMR experimental spectra at some temperatures in the SmA phase. The simulation was carried out by the Lequor program,[27] fixing the quadrupolar splitting $\Delta\nu_q$ and the line width to the values determined from the corresponding ^{1}H-decoupled spectra. The relevant dipolar coupling between the deuteron and the nearest aromatic proton was estimated by means of eq 1, using the S_{zz} value obtained from eq 2 with various trial values of Δ_{biax}. An estimate of the coupling between the deuteron and the protons of the first methylenic group of the alkoxylic chain was taken from the literature [30] and suitably scaled for the different nuclei involved in the interaction and for the different degree of orientational order. Good simulations of the spectra at some

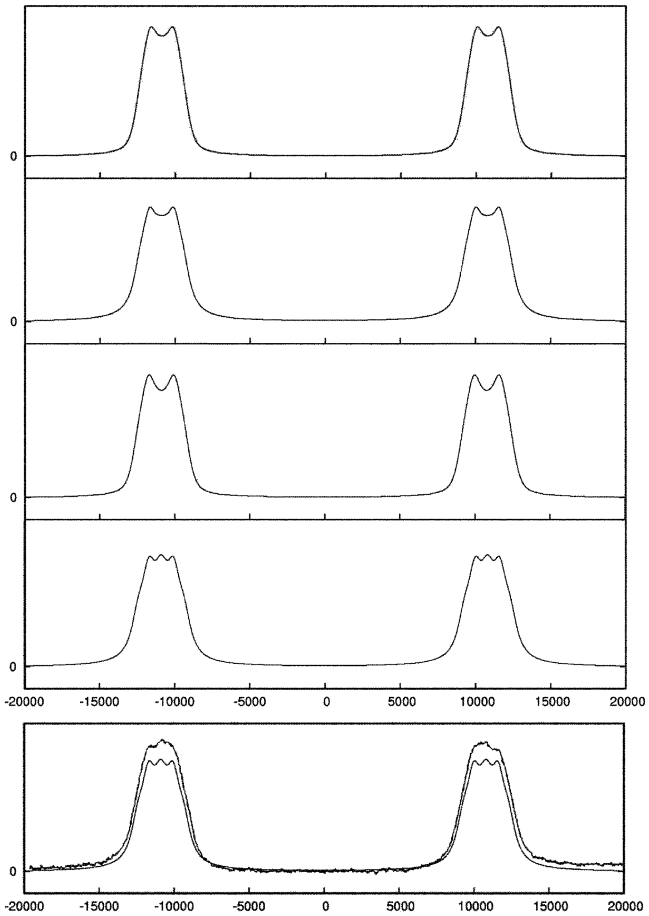

Figure 11. DNMR simulated spectra for ZLL 7/*-biphe-D2 in the SmA phase at 110 °C. From the top to the bottom: three spectra computed taking into account only the dipolar coupling between D and the nearest aromatic proton and $\Delta_{biax} = -0.01$, $\Delta_{biax} = 0$, $\Delta_{biax} = 0.01$; a spectrum computed taking into account also the dipolar couplings between D and the nearest methylenic protons and $\Delta_{biax} = 0$; comparison of the last simulated spectrum with the experimental one.

temperatures in the SmA phase were obtained only for $\Delta_{biax} \approx 0$, as shown in Figure 11 for $T = 110$ °C, where three spectra corresponding to different values of Δ_{biax} are compared to the experimental one. Accordingly to this finding, we have analyzed the quadrupolar splittings of **ZLL 7/*-biphe-D2**, fixing $\Delta_{biax} = 0$ at each temperature and directly computing $S_{zz}(T)$ from eq 2. Its worthwhile noting that the extrapolation of the condition $\Delta_{biax} = 0$ from the SmA to the other mesophases is rather arbitrary. The temperature dependence of the order parameter relative to the para axis of the biphenyl group is shown in Figure 10.

If the local *z* axis is well aligned to the "long" molecular axis (the best aligned to the local phase director), S_{zz} represents a good approximation of the molecular order parameter S^{mol}. For mesogenic molecules preferentially aligned along the magnetic field, as happens in the SmA phase, high values of S^{mol} are expected (0.6−0.8), together with low or vanishing molecular order biaxiality. [16,23] The S_{zz} values relative to the para axis of the two aromatic fragments are quite similar or coincident throughout the temperature range examined. We can conclude that the two para axes are mostly collinear.

Tilt Angles in Chiral Phases from DNMR Data. From the order parameters of Figure 10, the tilt angle θ in the chiral phases (SmC*, SmC*$_A$, SmC*$_{re}$, and hexatic) can be estimated.[16,23] In the magnetic field, such phases align with the helix axis parallel

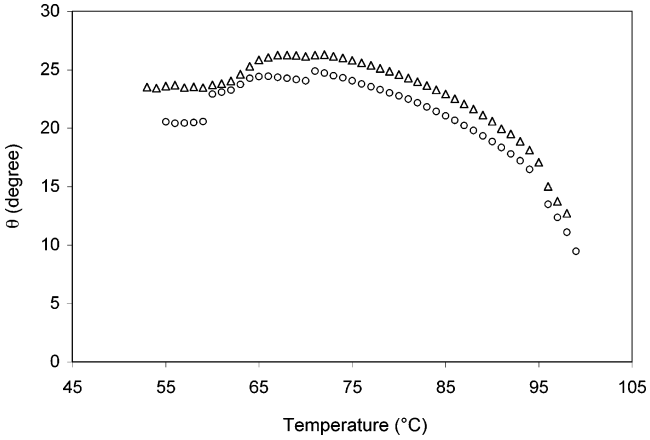

Figure 12. Tilt angle of the two labeled ZLL 7/* compounds vs temperature by DNMR. Triangles and circles refer to ZLL 7/*-biphe-D2 and ZLL 7/*-phe-D2, respectively.

to the field itself and the tilt angle θ coincides with the angle between the magnetic field and the local molecular director inside the smectic layers. Therefore, the following equation is valid:

$$S_{zz}^{H} = S_{zz}^{local}\left(\frac{3\cos^2\theta - 1}{2}\right) \qquad (3)$$

S_{zz}^{H} is the order parameter of a *z* axis fixed on the molecule, relative to the magnetic field direction, directly determined from the NMR experimental splittings, as previously described. S_{zz}^{local} is the order parameter relative to the local phase director, describing the average molecular orientation inside the smectic layer. S_{zz}^{local} coincides with S_{zz}^{H} and is therefore directly determined by the NMR experimental splitting whenever the local director aligns to the magnetic field, namely in the chiral phases unwound by the magnetic field itself, as in the uSmC* one.

For the SmC* phase of **ZLL 7/*-biphe-D2** and of **ZLL 7/*-phe-D2**, the order parameters of the *z* biphenyl and phenyl axis, respectively, are experimentally known both in the wound and unwound arrangement. Therefore, the evaluation of the tilt angle for each compound is straightforward and only requires reasonable presumption that the local order in the two arrangements is the same. For the other tilted mesophases (SmC*$_A$, SmC*$_{re}$, hexatic), S_{zz}^{local} is not experimentally known and must be inferred. In the case of **ZLL 7/*-biphe-D2**, the trend of S_{zz}^{local} relative to the uSmC* phase has been linerly extrapolated to low temperatures: the straight line obtained reaches the limit value $S_{zz}^{local} = 1$ just at the onset of the crystalline phase, as indicated in Figure 10. This fact supports the identification of the para axis of the biphenyl fragment with the "long" molecular axis. However, the procedure followed is mainly supported by the data relative to the mesogen MBHB: [25] in that case, a similar linear trend was experimentally found for the order parameter of the biphenyl para axis throughout the unwound uSmC* and uSmF* phases. Also, in the case of **ZLL 7/*-phe-D2**, the trend of S_{zz} relative to the uSmC* phase has been extrapolated to low temperature, pointing toward $S_{zz}^{local} = 1$.

The values of the θ tilt angle computed for the two samples are reported in Figure 12 as function of temperature. The tilt angles determined via DNMR are slightly but systematically higher for **ZLL 7/*-biphe-D2** than that for **ZLL 7/*-phe-D2**. The transition SmC*−SmC*$_A$ is marked by a sudden increase of θ, while the transition SmC*$_A$−SmC*$_{re}$ is marked by an

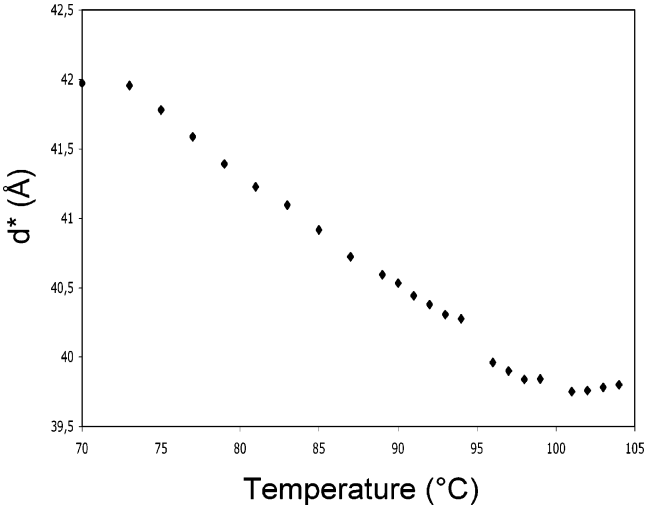

Figure 13. Layer spacing (Å) vs temperature (°C) of ZLL 7/*-phe-D2 corrected for the factor 1/cos(θ), where θ is the tilt angles evaluated from DNMR (see Figure 12). The four points between 100 and 105 °C indicate the experimental layer spacing in the SmA phase, taken from Figure 3.

opposite but less evident jump. Finally, the θ tilt angle is reduced in the hexatic phase.

Discussion and Conclusions

Ordering Effect of the Magnetic Field in the Chiral Phases. As described in the Quadrupolar and Dipolar Splittings, Line Widths, and Line Shapes vs Temperature section, the magnetic field has a peculiar effect on the ordering of the SmC* and SmC*$_{re}$ phases of both of the samples studied (see Figures 5−7).

In particular, the transition from the SmA phase, where the director is parallel to the magnetic field, to the SmC* phase, oriented with the helix axis parallel to the field, involves the formation of an uSmC* phase, in which the local molecular director is parallel to the magnetic field while the smectic layers are tilted. Such phase is thermodynamically unstable and always transforms into the SmC* one, except that in a temperature interval of 1−1.5 °C just below the transition from the SmA phase, in the 9.40 T magnetic field, where the most stable phase is the uSmC* one. The smectogen MBHB, already amply cited,[25] presented a similar behavior, with the difference that no coexistence between wound and unwound phases could be observed in that case. For MBHB, the occurrence of the sequence SmA−uSmC*−SmC* stable phases in the 7.05 T magnetic field and the disappearance of the uSmC* and SmC* phases at 4.70 T and 9.40 T, respectively, could be satisfactorily explained, minimizing of the Landau−de Gennes thermodynamic potential density. In this model, the term taking into account the magnetic field H is $g^H \cong -(1/2)\chi_a(H \cdot \cos\theta)^2$, where χ_a is the anisotropy of the molecular magnetic susceptivity, and θ is the tilt angle between H and the local molecular director. (Of course, there are other terms of the thermodynamic potential density also depending on θ). The formation of a stable uSmC* phase is possible above a critical value of the magnetic field, depending on the helix elastic constant and pitch and on the anisotropy of the molecular magnetic susceptivity. Also the behavior of the **ZLL 7/*** isotopomers can be explained on the basis of this model, provided that the critical field is just around 7.05 T and the formation of the uSmC* phase is the first step of the evolution from the SmA to the SmC* thermodynamically stable phase.

The situation is much more complex in the SmC*$_{re}$ phase, which forms between the SmC*$_A$ and the *hexatic* ones, both tilted. In this case, the line shapes recorded in the 7.05 and 9.40 T fields are drastically different (see Figure 6). In the lower field, a large and stable distribution of orientations is obtained. The minor splitting reported in Figure 5 denotes that a large fraction of the sample actually recovers the ordering behavior of the SmC* phase, but the relevant presence in the distribution of components corresponding to larger splittings indicates that another fraction of the sample settles in an ordering close to that of the impending *hexatic* phase. In the higher field, the narrow lines obtained indicate that, there, the phase orientation and structure is quite uniform. Because the magnetic field intensity should not substantially influence the rate of the reorienting processes in the sample, the explanation of these findings must be mainly based on static arguments. Therefore, in the 7.05 T magnetic field, the so-called *re-entrant* SmC* phase could be a temperature-dependent superimposition of chiral structures, with broad orientational distribution of the helix axes and different tilt angles. In the 9.40 T field, the angular distributions are substantially restricted, the helix structure uniform at each temperature, and the temperature dependence of the splitting ascribable to a continuous decrease of the tilt angle. The picture so outlined excellently fits the features typical of *frustrated* phases,[31] among which the *re-entrant* ones are located:[31] in these systems, different terms in the free energy expression dictate different molecular arrangements and the competition among these terms may result in quite complex and composite structures. The presence of the external magnetic field adds one more free energy term, which in the case of the 7.05 T field competes with the others without prevailing, while at 9.40 T becomes preponderant, imposing a homogeneous ordering of the directors.

A more detailed quantitative analysis is in progress.

Orientational Order Parameters and Structure. The orientational order parameters S_{zz} for the two deuterated fragments (the z axes are along the para axes), have been determined throughout the different mesophases. The S_{zz} values relative to the biphenyl fragment are quite similar to those of the phenyl fragment, thus indicating that the two para axes can be considered collinear and both well represent the direction of the long molecular axis. On the other hand, for similar compounds,[16,19] the aromatic fragment linked to the linear alkylic or alkoxylic chain is reported to reflect the molecular order better than the other aromatic moiety. The order parameter Δ_{biax} of the biphenyl fragment could be considered vanishing after the simulation of the line shape in the SmA phase, in full agreement with all the similar cases already studied.[16,19,25] It seems that uniaxial symmetry for the biphenyl moiety order matrix can be safely assumed in these kinds of compounds. The values of Δ_{biax} found for the phenyl fragment, ranging between 0.06 and 0.04 in the various smectic phases, are also quite similar to those reported in cited literature.

Tilt Angles in Chiral Phases. The tilt angles of the chiral phases have been determined with two quite different techniques for the two isotopomers, and the results reported in Figures 2 and 12 will be now compared. Altogether, the DNMR results of both **ZLL 7/*-biphe-D2** and **ZLL 7/*-phe-D2** are in excellent agreement with those obtained by optical measurements, with one remarkable difference: DNMR puts in evidence that the tilt angle across the SmC*$_A$ phase is slightly greater than that in the neighboring SmC* and SmC*$_{re}$ phases, while no discontinuity is found by the optical technique. This can be explained by recalling that the latter measurements are per-

formed on the phase unwound by an electric field perpendicular to the helix axis: such treatment is likely to cancel those differences between the SmC^*_A and SmC* phase properties that just reside in the peculiar helix winding.

Finally, we consider the temperature dependence of the layer spacing, reported in Figure 3. As briefly mentioned in the Layer Spacing Data paragraph, the trends observed with decreasing temperature reflect the increasing orientational order, the onset and variation of the tilt angle, and the effective variations of the layer thickness, three phenomena whose effects cannot be easily disentangled. However, we have attempted to "correct" the experimental layer spacing data $d(T)$ using the relation $d(T) = d^*(T)\cdot\cos\theta(T)$ and the tilt angles $\theta(T)$ determined by DNMR. The procedure has been limited to the data relative to **ZLL 7/*-phe-D2**, for which we have the X-ray data, and to the SmC* and SmC^*_A phases, whose microscopic tilted structure is certainly simpler and better known than that of the SmC^*_{re} and *hexatic* phases. The "corrected" layer thickness $d^*(T)$, shown in Figure 13, presents a marked discontinuity, or even a jump, at the onset of the SmC^*_A phase, and a rising trend across the SmC^*_A phase. The discontinuity or jump suggests that the $SmC^*-SmC^*_A$ transition could correspond to an effective elongation of the molecule due to a conformational change. In the literature, a conformational change has been often claimed to explain the occurrence of transitions between smectic phases, for instance, for the SmA−SmC* transition[32] or the SmA−SmC^*_A one, studied by ^2H and ^{13}C NMR.[29,33] As far as the $SmC^*-SmC^*_A$ transition is concerned, it was related to conformational changes in refs 34 and 35.

Acknowledgment. This work was financially supported by the P.R.I.N. 2003 (Italian MIUR), by Project COST D14 WG15; grant nos. 202/03/P011, 202/05/0431 from the Grant Agency of the Czech Republic. V.D. and A.B. acknowledge the financial support of STSM within COST Framework. We are grateful to Dr. D. Pociecha for the help with X-ray diffraction measurements, to Drs. M. Kaspar and V. Hamplova for supplying the ZLL 7/* compound, and to Prof. G. Galli for the help with optical microscope characterization.

References and Notes

(1) Kawamoto, S.; Oh-kochi, M.; Kundu, S.; Takatsu, H.; Kobayashi, S. *Displays* **2004**, *25*, 45.

(2) Chandani, A. D.; Gorecka, E.; Ouchi, Y.; Takezoe, H.; Fukuda, A. *Jpn J. Appl. Phys., Part 2* **1989**, *28*, L1265.

(3) Fukuda, A.; Takanishi, Y.; Isozaki, T.; Ishikawa, K.; Takezoe, H. *J. Mater. Chem.* **1994**, *3*, 997.

(4) Wrobel, S.; Haase, W. *Invited Lecture I15*, at the Ferroelectric Liquid Crystals Conference, Stare Jablonki, Poland, Sept 12−17, 2005.

(5) Cladis, P. E. *Phys. Rev. Lett.* **1975**, *35*, 48.

(6) Pociecha, D.; Gorecka, E.; Cepic, M.; Vaupotic, N.; Zeks, B.; Kardas, D. Mieckzowski, J. *Phys. Rev. Lett.* **2001**, *86*, 3048.

(7) Kaspar, M.; Hamplova, V.; Novotna, V.; Glogarova, M.; Pociecha, D.; Vanek, P. *Liq. Cryst.* **2001**, *28*, 1203.

(8) Novotna, V.; Glogarova, M.; Hamplova, V.; Kaspar, M. *J. Chem. Phys.* **2001**, *115*, 9036.

(9) Cladis, P. E. Re-entrant Phase Transitions in Liquid Crystals. In *Handbook of Liquid Crystals*; Demus, D., Goodby, J., Gray, G. W., Spiess, H. W., Vill, V., Eds.; WILEY-VCH: Weinheim, 1999; Chapter 6, pp 391−405.

(10) Musevic, I.; Blinc, R.; Zeks, B. *The Physics of Ferroelectric and Antiferroelectric Liquid Crystals*; World Scientific: Singapore, 2000.

(11) Marini, A.; Signore, G.; Menicagli, R.; Veracini, C. A. to be published.

(12) Veracini, C. A. NMR Spectra in Liquid Crystals the Partially Averaged Spin Hamiltonian. In *Nuclear Magnetic Resonance of Liquid Crystals*; Emsley, J. W., Ed.; Reidel: Dordrecht, 1985; Vol. 141, Chapter 5, p 99.

(13) Dong, R. Y. In *Nuclear Magnetic Resonance of Liquid Crystals*; Springer- Verlag: New York, 1997.

(14) Dong, R. Y. *Prog. Nucl. Magn. Reson.* **2002**, *41*, 115.

(15) Geppi, M.; Veracini, C. A. *Chiral Smectic Phases: NMR Studies*, *Encyclopedia of Nuclear Magnetic Resonance: Advances in NMR*; Grant, D. M., Harris, R. K., Eds.; John Wiley and Sons: Chichester, 2002; Vol. 9, pp 506−513.

(16) Catalano, D.; Chiezzi, L.; Domenici, V.; Geppi, M.; Veracini, C. A. *J. Phys. Chem. B* **2003**, *107*, 10104.

(17) Domenici, V.; Geppi, M.; Veracini, C. A.; Blinc, R.; Lebar, A.; Zalar, B. *ChemPhysChem* **2004**, *5*, 91.

(18) Catalano, D.; Cifelli, M.; Fodor-Csorba, K.; Gacs-Baitz, E.; Geppi, M.; Jakli, A.; Veracini, C. A. *Mol. Cryst. Liq. Cryst.* **2000**, *351*, 245.

(19) Catalano, D.; Cifelli, M.; Geppi, M.; Veracini, C. A. *J. Phys. Chem. A* **2001**, *105*, 34.

(20) Catalano, D.; Chiezzi, L.; Domenici, V.; Geppi, M.; Veracini C. A.; Dong, R. Y.; Fodor-Csorba, K. *Macromol. Chem. Phys.* **2002**, *203*, 1594.

(21) Chiezzi, L.; Domenici, V.; Geppi, M.; Veracini, C. A.; Dong, R. Y. *Chem. Phys. Lett.* **2002**, *358*, 257.

(22) Domenici, V.; Geppi, M.; Veracini, C. A. *Chem. Phys. Lett.* **2003**, *382*, 518.

(23) Catalano, D.; Cavazza, M.; Chiezzi, L.; Geppi, M.; Veracini, C. A. *Liq. Cryst.* **2000**, *27*, 621.

(24) Cifelli, M.; Domenici, V.; Veracini, C. A. *Mol. Cryst. Liq. Cryst.* **2005**, *429*, 167.

(25) Catalano, D.; Cifelli, M.; Domenici, V.; Fodor-Csorba, K.; Richardson, R.; Veracini, C. A. *Chem. Phys. Lett.* **2001**, *346*, 259.

(26) Luz, Z.; Meiboom, S. *J. Chem. Phys.* **1963**, *39*, 366.

(27) Diehl, P.; Kellerhals, H. P.; Niederberger, W. *J. Magn. Reson.* **1971**, *4*, 352.

(28) Yoshida, S.; Jin, B.; Takanishi, Y.; Tokumaru, K.; Ishikawa, K.; Takezoe, H.; Fukuda, A.; Kusumoto, T.; Nakai, T.; Miyajima, S. *J. Phys. Soc. Jpn.* **1999**, *68*, 9.

(29) Luckhurst, G. R.; Veracini, C. A. *The Molecular Dynamics of Liquid Crystals*; NATO ASI Series; Kluwer Academic Publishers: Boston, London, 1994.

(30) Emsley, J. W.; Celebre, G.; De Luca, G.; Longeri, M.; Catalano, D.; Veracini, C. A. *Gazz. Chim. Ital.* **1996**, *126*, 429.

(31) Crooker, P. P. *Liq. Cryst.* **1989**, *5*, 751.

(32) Photinos D. J.; Samulski, E. T. *Science* **1995**, *270*, 783.

(33) Fujimori, H.; Bayle, J. P.; Miyajima, S. *J. Phys. Soc. Jpn.* **2000**, *69*, 3090.

(34) Miyachi, K.; Matsushima, J.; Takanishi, Y.; Ishikawa, K.; Takezoe, H.; Fukuda, *A. Phys. Rev. E* **1995**, *52*, R2153.

(35) Wrzalik, R.; Merkel, K.; Kocot, A.; Cieplak, B. *J. Chem. Phys.* **2002**, *117*, 4889.